

From Cooper pair splitting to nonlocal spectroscopy of a Shiba state

Zoltán Scherübl^{1,2,3,*}, Gergő Fülöp^{1,2}, Jörg Gramich⁴, András Pályi⁵,
Christian Schönenberger⁴, Jesper Nygård⁶, and Szabolcs Csonka^{1,2}

¹*Department of Physics, Institute of Physics, Budapest University of Technology and Economics, Műegyetem rkp. 3., H-1111 Budapest, Hungary*

²*MTA-BME Nanoelectronics Momentum Research Group, Műegyetem rkp. 3., H-1111 Budapest, Hungary*

³*University Grenoble Alpes, CEA, Grenoble INP, IRIG, PHELIQS, 38000 Grenoble, France*

⁴*Department of Physics, University of Basel, Klingelbergstrasse 82, CH-4056 Basel, Switzerland*

⁵*Department of Theoretical Physics and MTA-BME Exotic Quantum Phases Research Group, Budapest University of Technology and Economics, H-1111 Budapest, Hungary*

⁶*Center for Quantum Devices and Nano-Science Center, Niels Bohr Institute, University of Copenhagen, Universitetsparken 5, DK-2100 Copenhagen, Denmark*



(Received 7 September 2021; revised 3 March 2022; accepted 8 April 2022; published 24 May 2022)

Cooper pair splitting (CPS) is a way to create spatially separated, entangled electron pairs. To this day, CPS is often identified in experiments as a spatial current correlation. However, such correlations can arise even in the absence of CPS, when a quantum dot is strongly coupled to the superconductor, and a subgap Shiba state is formed. Here, we present a detailed experimental characterization of those spatial current correlations, as the tunnel barrier strength between the quantum dot and the neighboring normal electrode is tuned. The correlation of the nonlocal signal and the barrier strength reveals a competition between CPS and the nonlocal probing of the Shiba state. We describe our experiment with a simple transport model and obtain the tunnel couplings of our device by fitting the model's prediction to the measured conductance correlation curve. Furthermore, we use our theory to extract the contribution of CPS to the nonlocal signal.

DOI: [10.1103/PhysRevResearch.4.023143](https://doi.org/10.1103/PhysRevResearch.4.023143)

I. INTRODUCTION

Cooper pair splitter devices were extensively studied both experimentally [1–8] and theoretically [9–19] in recent years. They are proposed to serve as the source of spatially separated entangled electron pairs. The standard Cooper pair splitter [see Fig. 1(a)] consists of a central superconducting electrode, which serves as the source of Cooper pairs, two normal leads, to which the split electron pair is transferred, and two quantum dots in between. The gate voltages of the quantum dots serve as the experimental knobs to tune the currents in the two different arms, utilizing the discrete energy spectrum of the dots.

Theoretically, several ways were proposed to test the performance of a Cooper pair splitter device, starting from current or noise correlations [20–22], through spin selective measurements [23–26] to proving the entanglement by demonstrating the violation of the Bell inequality [19,27–33] or using more complex spin-qubit or circuit quantum electrodynamics architectures [18,34,35] or even time domain measurements [36].

The experiments primarily focused on spatial current correlations [1–8]. In general, the currents flowing in the two arms are attributed to two different processes. The first process is the *local pair tunneling* (LPT), when both electrons of a Cooper pair are transferred to the same normal lead [see the black and green arrow on Fig. 1(a)]. This process involves only one arm of the device, and correspondingly it is independent of control parameters of the other arm. The second process is the Cooper pair splitting (CPS), when the two electrons end up in different normal electrodes [see the black and red arrows on Fig. 1(a)]. As both arms of the device are involved, the CPS process depends on the control parameters of both arms. Hence it results in a *nonlocal signal*, i.e., the current in one arm of the device is tuned by the control parameters (on-site energy (plunger gate voltage) and tunnel amplitude (barrier gate voltage)) of the other arm via tuning the CPS contribution.

In Ref. [37], we have shown that a nonlocal signal can be also present when the conductance of one of the arms of the Cooper pair splitter is quenched. It is achieved by isolating the quantum dot from its normal lead by a strong tunnel barrier. Since in this situation the CPS is forbidden, there must be another transport process that produces a nonlocal signal. This process emerges if the tunnel coupling between the superconductor and the isolated quantum dot is sufficiently strong, which gives rise to the formation of the Yu-Shiba-Rusinov (Shiba) state [38–41].

The subgap Shiba state is the result of the hybridization of the dot states and quasiparticle states of the

*scherubl.zoltan@gmail.com

Published by the American Physical Society under the terms of the [Creative Commons Attribution 4.0 International](https://creativecommons.org/licenses/by/4.0/) license. Further distribution of this work must maintain attribution to the author(s) and the published article's title, journal citation, and DOI.

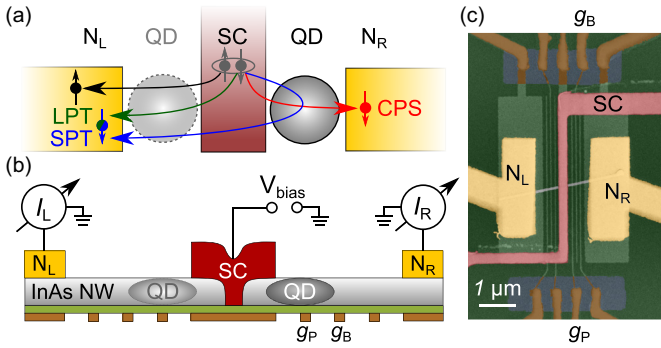


FIG. 1. (a) Schematics of a Cooper pair splitter. Cooper pairs are extracted from a central superconducting electrode (SC) to two normal leads (N_L and N_R), through quantum dots (QDs). The currents are built up of two contributions, the Cooper pair splitting (CPS, black and red arrows) and the local pair tunneling (LPT, black and green arrows). In the presence of a Shiba state at zero energy—if the SC and the QD are strongly coupled—a third process, the Shiba-assisted local pair tunneling (SPT, black and blue arrows) emerges. This produces a CPS-like nonlocal signal but does not create spatially separated electron pairs. The left QD is drawn with a dashed line, because it is not tuned throughout this work, but fixed as it only weakly transmits. [(b), (c)] Cross section and false color SEM image of the device. The InAs nanowire (NW) is placed on an array of bottom gate electrodes and contacted by the two normal and one superconducting electrode. The QD is formed in the NW, and tuned by the voltage on the plunger gate, g_P . The tunnel coupling to the N_R lead is tuned by the barrier gate, g_B .

superconductor and was extensively studied in a variety of hybrid nano devices [42–67]. They inherited their name from the subgap states in an analogous system, namely magnetic adatoms on a superconducting surface, which are widely studied by scanning tunneling microscope experiments [68–84]. We will call the transport mechanism responsible for the nonlocal signal in Ref. [37] *Shiba-assisted local pair tunneling* (SPT), since it is enabled by the Shiba state, and it involves subsequent transitions of two electrons (elements of a Cooper pair) into the same normal lead.

The experimental evidence of the SPT process, provided in Ref. [37], implies that a nonlocal signal in a Cooper pair splitter with strong superconductor-dot coupling is induced *together* by CPS and SPT. In turn, this implies that in general it is unjustified to interpret the entire nonlocal signal as CPS, and extra efforts are required to distinguish the contributions of CPS and SPT to the nonlocal signal. Here, we exemplify and illustrate this challenge by extending the analysis of the experimental data presented in Ref. [37], establish a theoretical framework allowing us to separate the two contributions, and show that the framework can indeed be successfully applied to our experiment, i.e., it separates the CPS and SPT contributions.

In the experiment [see Fig. 1(a) for the experimental setup, to be detailed below], we carried out transport measurements while the tunnel coupling between the quantum dot and the N_R lead was varied. Our transport model is based on the so-called zero bandwidth approximation (ZBA) for the superconductor [55,85–87]. Through our analysis, we find that close to the quenched regions (i.e., when the tunnel barrier toward N_R is

strong), a significant contribution of the nonlocal signal comes from the SPT process. Hence, in this parameter range, it is necessary to use our framework for a sound analysis. Since following earlier approaches, e.g., Refs. [1,2,5–7], attributing all of the nonlocal signal to CPS would overestimate the real CPS contribution in our case. We also show that in the case when the quantum dot of the Cooper pair splitter is well coupled to the N_R lead, the nonlocal signal dominantly comes from the splitting of Cooper pairs, and correspondingly the earlier approaches gives a reasonable result for the CPS contribution in that parameter range.

Our paper is structured as follows. In Sec. II, the device geometry and measurement techniques are introduced. In Sec. III, the experimental results are presented. We demonstrate the presence of a nonlocal signal for a wide range of parameters, we show a correlation between the local and the nonlocal signal, and we relate them to the Shiba state. In Sec. IV, the theoretical model and the transport calculation are introduced, and are used to fit the experimental data. In Sec. V, we discuss our findings, namely, the origin of the nonlocal signal and the correlation between the local and the nonlocal signal, we calculate the contributions of the CPS and SPT processes, and we discuss the validity of earlier splitting efficiency definitions. Finally, in Sec. VI, we conclude our findings.

II. DEVICE GEOMETRY

The Cooper pair splitter device is illustrated in Fig. 1. The schematics of the cross-section and a false-color SEM image of the device are shown in Figs. 1(b) and 1(c), respectively. The basis of the circuit is an InAs nanowire (NW), with a diameter of 70 nm, grown by gold catalyst assisted molecular beam epitaxy [88,89], using a two-step growth method to suppress the stacking faults [90]. First, an array of bottom gate electrodes (made of 4/18 nm Ti/Pt in brown) was defined by e-beam lithography and evaporation. The two outermost electrodes of the 9 are 1.3 μm wide and placed below the normal contacts. The middle electrode is 250 nm wide and placed below the superconductor. The remaining 3+3 electrodes are 30 nm wide with 100-nm period and serve to tune the electron density in the nanowire. The gate electrodes are covered by a 25 nm thick SiN_x layer (green), grown by plasma-enhanced chemical vapor deposition to electrically isolate the gates from the rest of the device. The SiN_x was removed by reactive ion etching with CHF_3/O_2 at the end of the gate electrodes to contact them [91]. The nanowire is contacted by two 4.5/100 nm thick Ti/Au normal electrodes (N_L and N_R in yellow) and a 4.5/110/20 nm thick Pd/Pb/In superconducting contact (SC in red) [92]. The nanowire was cut by focused ion beam prior to the deposition of the superconducting contact [see Fig. 1(b)] to suppress the direct tunnel coupling between the two arms of the device [93,94].

The differential conductance of the two arms were measured simultaneously with lock-in technique, using 10 μV AC signal on the superconducting contact at 237 Hz, on the two normal contacts by home-built current-voltage (I/V) converter. The measurements were carried out in a Leiden Cryogenics CF-400 top-loading cryo-free dilution refrigerator at a bath temperature of 35 mK. Prior to cooldown, the sample

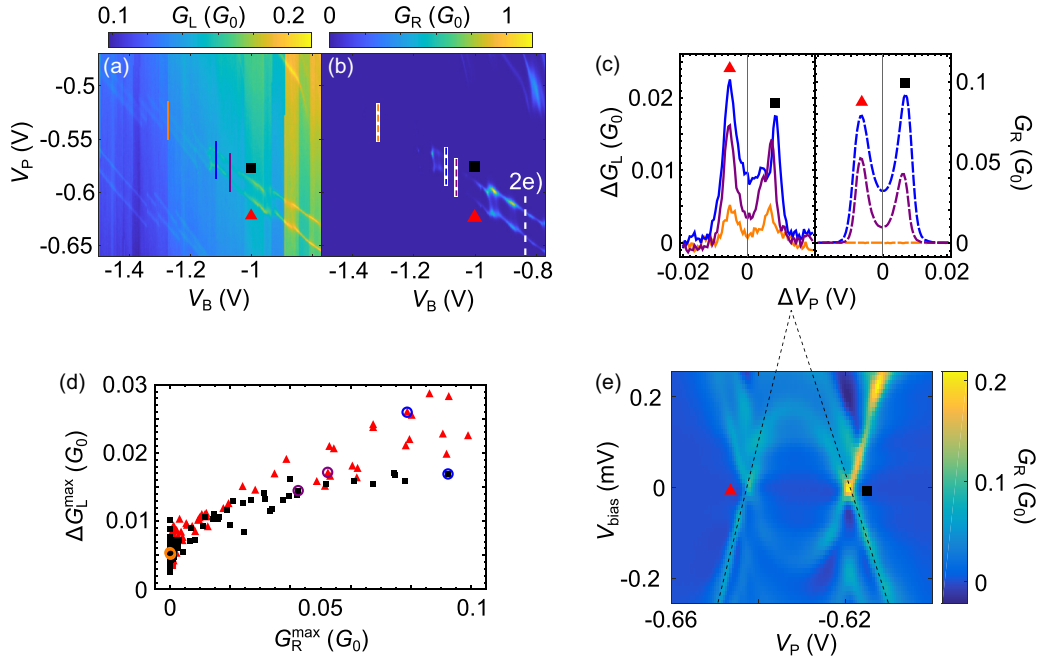


FIG. 2. [(a), (b)] Simultaneously measured zero-bias differential conductances of the two arms of the device, as the functions of the V_B (barrier) and V_P (plunger) gate voltages [37]. The quantum dot-like resonances of the right arm [marked with black square and red triangle in panel (b)] also appear in the conductance of the left arm (a). This nonlocal signal persists even when the conductance of the right arm is quenched. (c) Color-coded line cuts from panels (a) and (b) illustrating the correlation between the nonlocal signal in the left arm and the local conductance of the right arm. A gate-dependent background conductance is subtracted from each G_L curve. The conductance maxima values are extracted from each line cut along the resonances, as illustrated on panel (c) by the marks. These value pairs are plotted as a scatter plot in panel (d) to further demonstrate the correlation of the two conductances. The three particular example pairs of panel (c) are highlighted by color-coded circles. The nonlocal signal in the left arm increases with an increasing conductance of the right arm. (e) Finite-bias characterization of the quantum dot with open barrier, measured along the white dashed line on panel (b), at $V_B = -0.83$ V. The eye-shaped crossing is the signature of a Shiba state, which highlights the strong coupling between the superconductor and the quantum dot. The black dashed lines are used to estimate the charging energy to $U \approx 0.4$ meV [37].

was pumped overnight to remove the absorbed water from the surface of the nanowire.

III. EXPERIMENTAL RESULTS

The experimental results are summarized in Fig. 2. Figures 2(a) and 2(b) show the simultaneously measured zero-bias differential conductance (in units of $G_0 = 2e^2/h$) of the two arms of the Cooper pair splitter device, G_L and G_R , as the function of the gate voltages, V_B and V_P , which are applied on gate g_B and g_P , respectively. Note that both gate electrodes are placed under the *same* arm of the device [see Fig. 1(b)], and the left arm is not tuned, but fixed as it weakly transmits. Hence, contrary to usual Cooper pair splitters, instead of a quantum dot and a normal lead, the left arm can be considered as a tunnel coupled normal electrode. The barrier gate voltage, V_B , dominantly tunes the tunnel coupling to the N_R electrode, while V_P , the plunger gate voltage, tunes the level position of the quantum dot. The conductance G_R through the right arm [see Fig. 2(b)] is completely quenched for $V_B < -1.2$ V, while for more positive barrier gate voltages it starts to conduct along two parallel resonance lines (marked by a square and a triangle). This conduction pattern indicates a quantum dot-like behavior.

Remarkably, the two G_R resonances of the quantum dot also appear in the conductance G_L of the left arm [see

Fig. 2(a)] as a conductance enhancement on top of a smooth background. We will denote this conductance enhancement by ΔG_L , and call it the *nonlocal signal*. When the conductance of the right arm is finite ($V_B > -1.1$ V), the presence of this nonlocal signal is in agreement with previous measurements on Cooper pair splitters [1,2,5–7]. That is, when the quantum dot in the right arm is tuned to resonance, an additional transport channel opens, Cooper pairs are not only transferred to the left normal electrode by LPT processes, but they can be split between the two arms, and correspondingly increase the conductance of both arms. This $V_B > -1.1$ V regime of the data is qualitatively consistent with the picture of CPS.

However, the $V_B < -1.2$ V range of the data in Figs. 2(a) and 2(b) excludes the scenario that CPS is the only transport process inducing the nonlocal signal. There, the conductance G_R of the right arm is suppressed, but the nonlocal signal, i.e., the peaks in G_L , persists throughout the whole map. When G_R is quenched, the presence of the nonlocal signal cannot be attributed to the CPS anymore, since no electron can flow to the N_R electrode. Both electrons of the Cooper pairs have to leave to the left normal lead.

Furthermore, our data reveal that the amplitude of the nonlocal signal ΔG_L is controlled via the local conductance G_R . In other words, by tuning the rightmost barrier more transparent, the current moving in the left arm is also increased. This is illustrated in Fig. 2(c), by line cuts from 2(a)

and 2(b) along the color coded lines. The smooth background conductance is subtracted from each line cut of G_L and only the nonlocal signal, ΔG_L , is plotted. When G_R is quenched, the nonlocal signal goes up to about $\Delta G_L \approx 0.005 G_0$ [see the orange curves on Fig. 2(c), measured at $V_B = -1.281$ V]. As the local conductance increases, the amplitude of the nonlocal signal also increases (see the purple and blue curves, measured at $V_B = -1.098$ and -1.119 V, respectively). Note that G_R , and correspondingly the nonlocal signal also, varies in a nonmonotonic fashion as the barrier gate voltage is tuned; we attribute this to disorder in the sample.

The above-mentioned systematic relation of the local conductance G_R and the nonlocal signal ΔG_L is reinforced by the data shown in Fig. 2(d). Let us exemplify how we derive this data from the previous panels, using the line cuts in Fig. 2(c), focusing on the right maxima of the blue curves (marked by black squares). The maximum value of the nonlocal signal (left panel) is about $\Delta G_L^{\max} \approx 0.017 G_0$, while the maximum value of the local conductance (right panel) is $G_R^{\max} = 0.08 G_0$. These values give the vertical and horizontal coordinates of the corresponding data point in Fig. 2(d), respectively (see the black square highlighted by the blue circle). The other points of Fig. 2(d) were obtained similarly by reading the maxima of all vertical line cuts on Figs. 2(a) and 2(b). As Fig. 2(d) shows, even when the conductance of the right arm is quenched, i.e., $G_R^{\max} = 0$, the amplitude of the nonlocal signal is finite, residing between $0.002 G_0$ and $0.01 G_0$. As G_R is increased by lowering the barrier to the N_R lead, the nonlocal signal also increases in a monotonous, saturating fashion. Only data points with $G_R^{\max} < 0.1 G_0$ are shown in the figure. We choose this requirement to ensure the weak coupling to the right lead, which will be assumed in the modeling.

Using finite-bias measurements, we establish that the tunnel coupling between the superconducting lead and the quantum dot is strong, and hence a Shiba state is formed in the device. The finite-bias differential conductance measured along the white dashed line on Fig. 2(b) at $V_B = -0.83$ V is shown in Fig. 2(e). The eye-shaped crossing conductance lines are the usual signature of a Shiba state, formed in a strongly coupled superconductor–quantum dot hybrid (see, e.g., Ref. [54]). Correspondingly, the resonances Figs. 2(a) and 2(b) are the signatures of the zero-energy Shiba states rather than charge degeneracies of a quantum dot. These observations suggest that in our model of the device (see next section) we have to incorporate a strong, coherent hybridization between the superconductor and the quantum dot. Based on the finite-bias measurement shown in Fig. 2(e) the charging energy of the quantum dot can also be estimated, following the dashed lines, yielding $U \approx 0.4$ meV.

Our conclusion from this analysis is that when the conductance G_R of the right arm is quenched, the conductance enhancement ΔG_L of the left arm originates from the (zero-energy) Shiba state, i.e., the SPT mechanism, rather than the splitting of Cooper pairs. Hence, the conductance enhancement can be viewed as the nonlocal probing of the Shiba state. We analyzed this region in detail in Ref. [37].

In the following, we will use a simple model to explain the experimental findings, namely (i) the presence of the nonlocal signal when the right arm is quenched and (ii) the correlation

between the conductances when G_R is finite. We will model the Shiba state using the zero bandwidth approximation for the superconductor. This model will enable us to identify and separate contributions of the SPT and CPS processes [see Fig. 1(a)] to the nonlocal signal ΔG_L .

IV. MODEL

A. Zero-bandwidth approximation of the Shiba state

The Shiba state is formed by the hybridization of the quasiparticles of the superconductor and the quantum dot degrees of freedom induced by the strong tunnel coupling between the dot and the superconductor. A simple way to describe the Shiba state is by treating the superconductor using the zero bandwidth approximation (ZBA) [55,85–87]. In this approximation, the quasiparticles of the superconductor are restricted only to a discrete energy level at energy Δ , which can host 0, 1, or 2 quasiparticles. The corresponding Hamiltonian is

$$H_{\text{SC}}^{\text{ZBA}} = \Delta c_{\uparrow}^{\dagger} c_{\downarrow}^{\dagger} + \Delta c_{\downarrow} c_{\uparrow} = \Delta \sum_{\sigma} \gamma_{\sigma}^{\dagger} \gamma_{\sigma}, \quad (1)$$

where Δ is the superconducting gap, $c_{\sigma}^{(\dagger)}$ is the electron annihilation (creation) operator in the superconductor, and $\gamma_{\sigma}^{(\dagger)}$ is the annihilation (creation) operator of the quasiparticles, defined by the usual Bogoliubov transformation, $c_{\sigma} = \frac{1}{\sqrt{2}}(\gamma_{\sigma} - \sigma \gamma_{\bar{\sigma}}^{\dagger})$.

The quantum dot is described by the single-impurity Anderson Hamiltonian,

$$H_{\text{QD}} = \sum_{\sigma} \varepsilon n_{\sigma} + U n_{\uparrow} n_{\downarrow}, \quad (2)$$

where ε is the level position of the dot, U is the charging energy, and $n_{\sigma} = d_{\sigma}^{\dagger} d_{\sigma}$ is the number of the electrons with spin σ on the dot, with $d_{\sigma}^{(\dagger)}$ being the annihilation (creation) operator of electrons with spin σ on the dot. Note that compared to the usual Cooper pair splitter geometry, where quantum dots are placed on both side of the superconductor [as illustrated in Fig. 1(a)], in this model we only consider the dot of the right arm. Since in the experiment the left arm of the device was not tuned but fixed in a weakly transmitting region, the left normal electrode and the left dot is modeled as a tunnel coupled normal lead for simplicity [see Fig. 3(a) and Sec. IV B].

The tunnel coupling between the superconductor and the dot is described by

$$H_{\text{TS}} = t_{\text{S}} \sum_{\sigma} (d_{\sigma}^{\dagger} c_{\sigma} + c_{\sigma}^{\dagger} d_{\sigma}). \quad (3)$$

Using the Bogoliubov transformation above, this translates to

$$H_{\text{TS}} = \frac{1}{\sqrt{2}} \sum_{\sigma} t_{\text{S}} [d_{\sigma}^{\dagger} (\gamma_{\sigma} - \sigma \gamma_{\bar{\sigma}}^{\dagger}) + (\gamma_{\sigma}^{\dagger} - \sigma \gamma_{\bar{\sigma}}) d_{\sigma}]. \quad (4)$$

The composite system of the superconductor and the quantum dot is hence modeled by $H_{\text{SC}}^{\text{ZBA}} + H_{\text{QD}} + H_{\text{TS}}$. A natural basis of the corresponding 16-dimensional Fock space is the product basis of the electron Fock space of the QD and the quasiparticle Fock space of the superconductor, that is, the basis $|i, j\rangle = |i\rangle_{\text{QD}} \otimes |j\rangle_{\text{SC}}$. Here, $\{|0\rangle_{\text{QD}}, |\uparrow\rangle_{\text{QD}}, |\downarrow\rangle_{\text{QD}}, |\uparrow\downarrow\rangle_{\text{QD}}\}$ is the canonical basis of the electron Fock space of the QD and

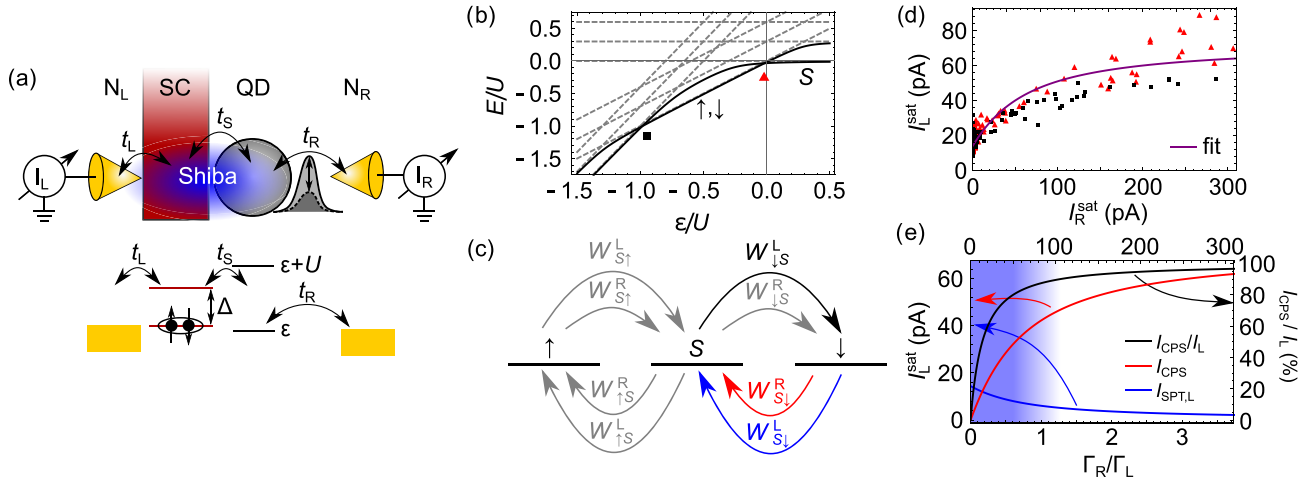


FIG. 3. (a) Schematics (top) and energy diagram (bottom) of our model. The tunnel coupling t_S between the superconductor (SC) and quantum dot (QD) creates a Shiba state (in blue). The normal leads, N_L and N_R , probe the Shiba state with coupling strength t_L and t_R , respectively. For simplicity, the SC is treated within the zero bandwidth approximation, in which the quasiparticles are restricted to a discrete energy level at Δ energy. (b) Illustrative energy spectrum of the QD–SC hybrid as the function of the dot’s level position ε . Gray dashed lines are the energies of the uncoupled system, while the black continuous lines are the possible ground states of the coupled system, the *singlet* (S) and the *doublets*, (\uparrow , \downarrow). The ground-state transitions are marked with red triangle and the black square in accordance with Fig. 2. (c) Illustration of the dynamics induced by the coupling to the normal leads. The tunneling induces transitions between the different ground states of the dot–superconductor system, the singlet and the doublets. The highlighted, colored arrows illustrate the tunnel processes shown on Fig. 1(a). (d) Fitting the experimental data with the ZBA model. Purple line is the fit with $t_S = 0.145$ meV, $\Gamma_L = 1$ μ eV, and $\Gamma_R = 0\text{--}3.6$ μ eV. (e) Contribution of the CPS (red) and the SPT (blue) processes to the nonlocal signal of the left arm and the relative ratio of the CPS processes (black). In the shaded blue region, the nonlocal signal is not a good measure of the CPS, since the SPT contribution is not negligible.

$\{|0\rangle_{SC}, |\uparrow\rangle_{SC}, |\downarrow\rangle_{SC}, |\uparrow\downarrow\rangle_{SC}\}$ is the canonical basis of the quasiparticle Fock space of the superconductor. The basis states are eigenstates of the uncoupled QD–superconductor system, i.e., of $H_{SC}^{\text{ZBA}} + H_{QD}$. The energy spectrum of the uncoupled system is illustrated on Fig. 3(b) with gray dashed lines as the function of the dot’s level position, ε . The three different slopes correspond to the different fillings of the dot, while from the parallel lines the bottom one corresponds to zero, the middle one to one, and the top one to two quasiparticles in the superconductor. The product basis can be partitioned to states with even fermion-number parity and odd fermion-number parity, the two subset of basis states spanning the even-parity and odd-parity sectors (subspaces), respectively.

The tunnel coupling H_{TS} hybridizes the states within each parity sector in two ways. First, it converts a quasiparticle from the superconductor to an electron on the dot (or the other way around), and second, it splits a Cooper pair to an electron on the dot and to a quasiparticle in the superconductor (or the other way around). Note that although the latter process does preserve the fermion-number parity, it does not preserve the fermion number.

The eigenstates of the coupled superconductor–quantum dot system can be grouped into six invariant subspaces, which can be labeled by the total spin of the electrons and the quasiparticles. The five-dimensional spinless, *singlet* (S) sector is spanned by the states $\{|0, 0\rangle, |\uparrow\downarrow, 0\rangle, |0, \uparrow\downarrow\rangle, |\uparrow\downarrow, \uparrow\downarrow\rangle\}$, and the state $\frac{1}{\sqrt{2}}(|\uparrow, \downarrow\rangle - |\downarrow, \uparrow\rangle)$. In the absence of magnetic field, the eight states with odd number of fermions can be grouped into two subspaces. The states $\{|\uparrow, 0\rangle, |0, \uparrow\rangle, |\uparrow\downarrow, \uparrow\rangle, |\uparrow, \uparrow\downarrow\rangle\}$ ($\{|\downarrow, 0\rangle, |0, \downarrow\rangle, |\uparrow\downarrow, \downarrow\rangle, |\downarrow, \uparrow\downarrow\rangle\}$) form the twofold degener-

ate *doublet* (D) subspaces. These states have $+1/2$ ($-1/2$) spin z component. The remaining three triplet states are uncoupled from the other states and from each other.

To model our Shiba-related transport measurement results, only the lowest energy singlet and doublet states are required. The former one (latter ones) will be denoted by $|S\rangle$ ($|\sigma\rangle$), with $\sigma \in \{\uparrow, \downarrow\}$. These states are illustrated on Fig. 3(b) as black lines.

B. Transport calculation

In the experiment, the system is simultaneously probed by two tunnel-coupled normal electrodes, as illustrated in Fig. 3(a). The tunnel coupling to the normal leads are described by

$$\begin{aligned} H_{TL} &= t_L \sum_{\sigma} (c_{L\sigma}^{\dagger} c_{\sigma} + c_{\sigma}^{\dagger} c_{L\sigma}) \\ &= \frac{t_L}{\sqrt{2}} \sum_{\sigma} [c_{L\sigma}^{\dagger} (\gamma_{\sigma} - \sigma \gamma_{\bar{\sigma}}^{\dagger}) + (\gamma_{\sigma}^{\dagger} - \sigma \gamma_{\bar{\sigma}}) c_{L\sigma}], \\ H_{TR} &= t_R \sum_{\sigma} (c_{R\sigma}^{\dagger} d_{\sigma} + d_{\sigma}^{\dagger} c_{R\sigma}), \end{aligned} \quad (5)$$

where $c_{L/R\sigma}^{(\dagger)}$ are the annihilation (creation) operators of the electrons in the left-right normal leads. The left lead couples only to the superconductor, while the right one couples only to the quantum dot.

As stated above, the Hamiltonian of the superconductor–quantum dot system, $H_{SC}^{\text{ZBA}} + H_{QD} + H_{TS}$, preserves the parity of the system, while the tunnel coupling to the normal leads induces transitions between eigenstates with different parity while transferring individual electrons to the normal leads.

These transitions are illustrated in Fig. 3(c) and described in the following.

For simplicity, we assume zero temperature, a gate-voltage configuration enabling resonant tunneling, i.e., that $E_S = E_\sigma$ for the energy eigenvalues of the singlet and double ground states and that a small negative bias voltage is applied on the superconducting lead, to ensure that electrons flow only toward the normal leads. Note that the resonant-tunneling condition is satisfied for two different on-site energies, in the vicinities of $\varepsilon = 0$ and $\varepsilon = -U$, respectively, and our approach described here is valid for both configurations.

Since the tunnel couplings to the normal leads were kept weak in the experiment, we treated the electron transport to the normal leads perturbatively, using Fermi's golden rule. The nonzero transition rates are

$$\begin{aligned} W_{S\sigma}^L &= \frac{\Gamma_L}{\hbar} \left| \langle S | \frac{\gamma_\sigma - \sigma \gamma_\sigma^\dagger}{\sqrt{2}} | \sigma \rangle \right|^2, \\ W_{\sigma S}^L &= \frac{\Gamma_L}{\hbar} \left| \langle \sigma | \frac{\gamma_\sigma - \sigma \gamma_\sigma^\dagger}{\sqrt{2}} | S \rangle \right|^2, \\ W_{S\sigma}^R &= \frac{\Gamma_R}{\hbar} |\langle S | d_\sigma | \sigma \rangle|^2, \\ W_{\sigma S}^R &= \frac{\Gamma_R}{\hbar} |\langle \sigma | d_\sigma | S \rangle|^2, \end{aligned} \quad (6)$$

where $\Gamma_{L/R} = \pi \rho_{L/R} t_{L/R}^2$ is the coupling to the left-right normal lead with $\rho_{L/R}$ being the density of state of lead $N_{L/R}$. The *f/i* indices of $W_{fi}^{L/R}$ denote the *final/initial* states of the given transition. The transition matrix elements are calculated at the ε values, where the singlet and doublet ground states are degenerate as in the measurement, outlined in Sec. III.

The tunnel coupling to the normal leads induces parity changing transitions between the different states of the superconductor–quantum dot hybrid as illustrated in Fig. 3(c). For example, the black arrow denotes the tunneling event, which brings the system from the $|S\rangle$ state to the $|\downarrow\rangle$ state, while an electron is transferred to the N_L lead. The time evolution of the occupation probabilities of the $|S/\sigma\rangle$ states, $P_{S/\sigma}$ is described by a classical master equation,

$$\begin{aligned} \frac{dP_S}{dt} &= \sum_\sigma [(W_{S\sigma}^L + W_{S\sigma}^R)P_\sigma - (W_{\sigma S}^L + W_{\sigma S}^R)P_S], \\ \frac{dP_\sigma}{dt} &= (W_{\sigma S}^L + W_{\sigma S}^R)P_S - (W_{S\sigma}^L + W_{S\sigma}^R)P_\sigma, \end{aligned} \quad (7)$$

together with the normalization condition $P_S + \sum_\sigma P_\sigma = 1$.

After determining the stationary solution ($dP_i/dt = 0$) of the master equation, the current in lead $N_{L/R}$ is given by

$$I_{L/R} = e \sum_\sigma (W_{\sigma S}^{L/R} P_S + W_{S\sigma}^{L/R} P_\sigma). \quad (8)$$

C. Comparison of the experiment and the theory

To compare the experimentally measured differential conductances to the calculated currents, one should find a relation connecting them. A naive way would be assuming a linear relation and simply using the $10 \mu\text{V}$ amplitude of the AC bias voltage for the conversion, i.e., $I_{L/R}^{\text{AC}} = G_{L/R} \times 10 \mu\text{V}$. However, while the calculation results in a zero-width con-

ductance peak, in the experiment the peak is broadened, and therefore the naive way strongly underestimates the saturation DC current at high bias. We estimate the saturation current using the zero-bias data in the following way. We estimate the broadening of the peaks by converting the width of the gate-dependent resonance curves measured at zero bias [see, e.g., Fig. 2(c)] using the lever arm, determined from the finite bias measurement on Fig. 2(e). This yields about $50 \mu\text{eV}$ width, barely varying with V_B . Assuming a Lorentzian shape for the resonance with this width the ratio of the saturation DC current and the zero-bias AC current is

$$\frac{I_{L/R}^{\text{sat}}}{I_{L/R}^{\text{AC}}} = \frac{\int_0^\infty G_{L/R}(V) dV}{G_{L/R}(V=0)V_{\text{AC}}} \approx 4. \quad (9)$$

In the following, we use this relation to convert the measured zero-bias differential conductances to saturated currents.

We used the framework detailed above to fit our experimental data. The charging energy and the superconducting gap is fixed to the experimental value of $U = 0.4 \text{ meV}$ and $\Delta = 0.25 \text{ meV}$, respectively. As ε is fixed by the degeneracy condition, only t_S remains a free parameter in the model of the coupled superconductor and QD. In the following, we will focus first on the degeneracy point near $\varepsilon = 0$, i.e., the 0-1 transition of the dot. Our results can be directly translated to the other degeneracy point, using symmetry arguments. Besides t_S , which determines the transition matrix elements, the couplings to the normal leads, Γ_L and Γ_R , are also fitting parameters of the model. Note that Γ_R is tuned in the experiment, and therefore the fitting does not give a single value but a range starting from zero. Therefore, the fitting parameter is not Γ_R itself, but its maximal value Γ_R^{max} .

The fitted curve is shown in Fig. 3(d) with the purple line, using $t_S = 0.145 \text{ meV}$, $\Gamma_L = 1 \mu\text{eV}$, and $\Gamma_R = 0 - 3.6 \mu\text{eV}$. The fit captures well the main features of the experiment. First, the model reproduces the finite current in the left lead even when the conductance of the right arm is quenched. Second, G_L also increases as G_R is enhanced by the increasing Γ_R . Third, the model gives a saturating tendency for the nonlocal signal as the barrier to the right lead is opened up. Note that the precise values of the fitted parameters may slightly vary when one or the other assumption used during the evaluation is relaxed, but the qualitative behavior remains unchanged.

V. DISCUSSION

Previously we demonstrated that the ZBA model of the Shiba state well reproduces our experimental findings: (i) the presence of the nonlocal signal, even when G_R is quenched, and (ii) the correlation between the height of the local and the nonlocal conductance peaks. The model allows for the detailed understanding of the experimental features, and furthermore, it can distinguish between the SPT and CPS contribution of the currents.

First, we have to discuss why the Shiba language (i.e., treating the superconductor–quantum dot hybrid as a coherently coupled unit) is necessary to describe our measurements. Often in Cooper pair splitters the electron transition between the superconductor and quantum dots is also described by tunnel rates, derived in a perturbative model, which assumes weak tunnel couplings [1,2,6]. In our measurements, the

presence of the eye-shaped subgap resonances in Fig. 2(e) implies that the tunnel coupling t_S between the superconductor and the quantum dot is comparable to the value of the gap (which we also verified by the fit, $t_S = 0.145$ meV). Therefore, it cannot be treated perturbatively, but the coherent hybridization of the superconductor and the dot has to be taken into account. Considering the usual perturbative description of the Cooper pair splitters, the presence of the nonlocal signal in the region, where G_R is zero, is surprising, since the process, which can generate a nonlocal signal—the CPS—is forbidden. However, in the Shiba description, this nonlocal signal is naturally present, as we will see below.

Second, we observed that the amplitude of the nonlocal signal increases as G_R is increased by enhancing the tunnel coupling to the N_R lead. This correlation is a result of a bottleneck effect. When the right lead is isolated from the rest of the device, all electrons have to leave to the N_L lead. This means that both the *singlet*→*doublet* and the *doublet*→*singlet* transitions must occur, involving a tunneling to the left lead. If the transition rates are much different, the slower one creates a bottleneck. Indeed, using the model parameters obtained by the fit, one finds that $\hbar W_{S\sigma}^L \approx 0.036$ μeV [the blue and the top left gray arrow on Fig. 3(c)] and $\hbar W_{\sigma S}^L \approx 0.191$ μeV [the black and the bottom left gray arrow on Fig. 3(c)]. The former rate is more than five times smaller than the latter one, i.e., the left current is limited by the *doublet*→*singlet* transition. However, opening up the barrier to the right lead opens up another transport channel for the slower process. As the $W_{S\sigma}^R$ rate becomes larger than $W_{\sigma S}^L$, the *doublet*→*singlet* process happens more favorably by transferring an electron to the right lead, and the bottleneck starts to be resolved. Although the presence of the new transport channel first means that not all the electrons are transferred to the left lead (which would mean the decrease of the nonlocal signal), but the whole transport sequence speeds up so much that altogether the left current increases.

The presence of nonlocal signals was reported previously in Cooper pair splitters hosting superconducting subgap states [53,57]. The authors used the infinite superconducting gap limit description—frequently referred as Andreev bound states—to model their experimental results. Using this approximation, all transition matrix elements contain the d -operators' matrix elements, and therefore the ratio of the left rates and the right rates are the same, i.e., $W_{\sigma S}^L/W_{S\sigma}^L = W_{\sigma S}^R/W_{S\sigma}^R$. With a simple derivation it can be shown that increasing Γ_R cannot resolve the bottleneck effect, since it drops out of the formula of I_L . Here, first we introduce how these processes are defined based on single tunneling events, and then we calculate their contribution.

The whole transport consists of a sequence of *singlet*→*doublet* and *doublet*→*singlet* transitions. Assuming that one starts from the singlet ground state, the transport can be grouped into a random sequence of SPT and CPS processes. Let us illustrate this using Fig. 3(c). The highlighted arrows indicate a CPS and a SPT process. Starting from the singlet ground state, let us assume that first an electron (with up spin) is transferred to the left lead. This is indicated by the black arrow. At the end of the tunneling event, the superconductor–quantum dot hybrid system stays in the $|\downarrow\rangle$ state. To return to the singlet state, there are two

possibilities. First, a second electron (with down spin) leaves to the left lead also (indicated by the blue arrow), and second, this electron is transferred to the right lead (red arrow). In the first process, two electrons with opposite spins are transferred to the *same* lead, and therefore a SPT event occurred, while in the second process the two electrons end up in *different* leads, corresponding to a CPS process. As the system returned to the singlet state, the transport cycle starts again.

The contribution of the CPS and SPT processes can be calculated within the framework of our model. Substituting the stationary solution of the master equation (7) to the expression of the currents, Eq. (8), one finds that the currents can be partitioned as

$$I_{L/R} = I_{\text{SPT,L/R}} + I_{\text{CPS}} \quad (10)$$

where

$$I_{\text{SPT,L/R}} = A \sum_{\sigma} 2W_{S\sigma}^{L/R} W_{\sigma S}^{L/R} \quad (11)$$

is the SPT contribution and

$$I_{\text{CPS}} = A \sum_{\sigma} (W_{S\sigma}^L W_{\sigma S}^R + W_{S\sigma}^R W_{\sigma S}^L) \quad (12)$$

is the CPS one. In $I_{\text{SPT,L/R}}$ the factor of 2 indicates that both electrons are transferred to the same lead, and the normalization factor is $A = 4e[\sum_{\sigma} (W_{S\sigma}^L + W_{S\sigma}^R + 2W_{\sigma S}^L + 2W_{\sigma S}^R)]^{-1}$. Note that to obtain these formulas, the spin rotational symmetry was used, which implies the spin independence of the transition rates, e.g., $W_{S\uparrow}^L = W_{S\downarrow}^L$. We should remind the reader that the presented model does not account for the LPT process, as it is independent of the Shiba state, consisting only of Cooper pairs tunneling from the superconductor directly to the normal lead.

This separation of I_L using the obtained fit parameters is plotted in Fig. 3(e). The CPS and SPT contributions are plotted in red and blue, respectively [the total current is shown in Fig. 3(c) in purple], and furthermore the CPS efficiency is plotted in black, which depends only on the Γ_R/Γ_L ratio for fixed t_S , not on their values. When $G_R = 0$ the splitting of Cooper pairs is forbidden, since no electrons can be transferred to the right lead. Accordingly, the CPS contribution is zero. The total current in the left lead comes only from the SPT process. This limit corresponds to the nonlocal spectroscopy of the Shiba state [$V_B < -1.2$ V region on Fig. 2(a)]. As the conductance of the right arm is increased, the amplitude of the SPT processes decreases while the CPS one strongly increases. When the barrier to the right lead is transparent, about 95% of the nonlocal signal comes from CPS processes. This is the usual Cooper pair splitter limit [$V_B > -1.1$ V region on Figs. 2(a) and 2(b)].

In between the two limits, there is a region where a significant contribution of the nonlocal signal comes from SPT processes, and this is indicated by the blue shaded region. In this region, the usual splitting efficiencies, which assume that the nonlocal signal comes only from the splitting of Cooper pairs, overestimate the real contribution of CPS processes.

Our results can be generalized to the conventional Cooper pair splitter geometry, i.e., the N–QD–SC–QD–N setup, in a straightforward way. The strongly coupled QD–SC–QD system hosting Andreev or Shiba molecular states was recently

studied in Refs. [95] and [96]. Similarly to the presented model, in these systems the ground state can be either a unique singlet or a twofold degenerate doublet and currents can flow to the normal leads when all of these three states are degenerate. Therefore, the transport processes illustrated in Fig. 3(c) and the partitioning of the currents, presented in Eqs. (10)–(12), also applies to the conventional splitter setup. The transport data measured in such a setup can be evaluated analogously to obtain the microscopic parameters and to partition the currents, and only the transition matrix elements have to be derived from the N–QD–SC–QD–N setup’s Hamiltonian.

In conclusion, close to the quenched regime a significant contribution of the nonlocal signal comes from the SPT processes, but in the transparent barrier limit the nonlocal signal provides a good measure of the CPS processes.

VI. CONCLUSIONS

We have investigated the nonlocal signal of a Cooper pair splitter as the tunnel coupling to one of the normal leads was varied. It was shown that the nonlocal signal persists even upon quenching the conductance in the opposite arm of the splitter, contradicting the expectations since in this limit the CPS process is forbidden. We resolved the contradiction by considering the Shiba state, originating from the hybridization of the quantum dot and the superconductor states. In the quenched limit, the nonlocal signal is attributed to the largely extended zero-energy Shiba state, which we studied in detail in Ref. [37].

The unexpected nonlocal signal we observed implied that figures of merit for Cooper pair splitting efficiencies used in previous experimental works could not be applied for our device. Therefore, we constructed a transport model using the ZBA for the superconductor to reproduce our experimental findings and to separate the Shiba related nonlocal signal from the CPS. Despite of its simplicity, the model captures well the main features of the experiments. Utilizing the model and the

obtained microscopic parameters we showed that closed to the quenched region, the nonlocal signal mostly consists of the SPT process, and therefore, the previously applied efficiency indicators overestimate the real CPS contribution. However, when the tuned barrier is transparent, the nonlocal signal is dominated by the CPS process, and accordingly, our results are consistent with those based on the standard CPS efficiency indicators.

The data that underlie the plots within this paper and other findings of this study are available in Ref. [97].

ACKNOWLEDGMENTS

We acknowledge Morten H. Madsen for MBE growth, Titusz Fehér, Péter Makk, Cătălin Pașcu Moca, Pascal Simon, Attila Virosztek, and Gergely Zaránd for useful discussions. We also acknowledge SNI NanoImaging Lab for FIB cutting, and M. G. Beckerné, F. Fülöp, and M. Hajdú for their technical support. This research was supported by the Ministry of Innovation and Technology and the National Research, Development and Innovation Office within the Quantum Information National Laboratory of Hungary and by the Quantum Technology National Excellence Program (Project Nr. 2017-1.2.1-NKP-2017-00001), by the NKFIH fund TKP2020 IES (Grant No. BME-IE-NAT), and by the OTKA Grant No. 132146 and K138433, by QuantERA SuperTop project 127900, by AndQC FetOpen project, by SuperGate FetOpen project, by NanocoHybri COST Action CA16218, and by the Danish National Research Foundation. C.S. acknowledges support from the Swiss National Science Foundation through Grants No. 192027, the NCCR QSIT, NCCR SPIN, and the QuantERA project SuperTop. C.S. further acknowledges support from the European Union’s Horizon 2020 research and innovation programme through Grant Agreement No. 828948, Project AndQC. G.F. acknowledges Bolyai János Scholarship and was supported by the ÚNKP-21-5 New National Excellence Program of the Ministry for Innovation and Technology from the source of the National Research, Development and Innovation Fund.

-
- [1] L. Hofstetter, S. Csonka, J. Nygård, and C. Schönenberger, Cooper pair splitter realized in a two-quantum-dot Y-junction, *Nature (London)* **461**, 960 (2009).
 - [2] L. G. Herrmann, F. Portier, P. Roche, A. L. Yeyati, T. Kontos, and C. Strunk, Carbon Nanotubes as Cooper-Pair Beam Splitters, *Phys. Rev. Lett.* **104**, 026801 (2010).
 - [3] J. Wei and V. Chandrasekhar, Positive noise cross-correlation in hybrid superconducting and normal-metal three-terminal devices, *Nat. Phys.* **6**, 494 (2010).
 - [4] L. Hofstetter, S. Csonka, A. Baumgartner, G. Fülöp, S. d’Hollós, J. Nygård, and C. Schönenberger, Finite-Bias Cooper Pair Splitting, *Phys. Rev. Lett.* **107**, 136801 (2011).
 - [5] A. Das, Y. Ronen, M. Heiblum, D. Mahalu, A. V. Kretinin, and H. Shtrikman, High-efficiency Cooper pair splitting demonstrated by two-particle conductance resonance and positive noise cross-correlation, *Nat. Commun.* **3**, 1165 (2012).
 - [6] J. Schindele, A. Baumgartner, and C. Schönenberger, Near-Unity Cooper Pair Splitting Efficiency, *Phys. Rev. Lett.* **109**, 157002 (2012).
 - [7] Z. B. Tan, D. Cox, T. Nieminen, P. Lähteenmäki, D. Golubev, G. B. Lesovik, and P. J. Hakonen, Cooper Pair Splitting by Means of Graphene Quantum Dots, *Phys. Rev. Lett.* **114**, 096602 (2015).
 - [8] S. Baba, C. Jünger, S. Matsuo, A. Baumgartner, Y. Sato, H. Kamata, K. Li, S. Jeppesen, L. Samuelson, H. Q. Xu, C. Schönenberger, and S. Tarucha, Cooper-pair splitting in two parallel InAs nanowires, *New J. Phys.* **20**, 063021 (2018).
 - [9] G. B. Lesovik, T. Martin, and G. Blatter, Electronic entanglement in the vicinity of a superconductor, *Eur. Phys. J. B* **24**, 287 (2001).
 - [10] P. Recher, E. V. Sukhorukov, and D. Loss, Andreev tunneling, Coulomb blockade, and resonant transport of nonlocal spin-entangled electrons, *Phys. Rev. B* **63**, 165314 (2001).

- [11] J. Eldridge, M. G. Pala, M. Governale, and J. König, Superconducting proximity effect in interacting double-dot systems, *Phys. Rev. B* **82**, 184507 (2010).
- [12] B. Hiltcher, M. Governale, J. Splettstoesser, and J. König, Adiabatic pumping in a double-dot Cooper-pair beam splitter, *Phys. Rev. B* **84**, 155403 (2011).
- [13] M. Leijnse and K. Flensberg, Coupling Spin Qubits via Superconductors, *Phys. Rev. Lett.* **111**, 060501 (2013).
- [14] M. Veldhorst and A. Brinkman, Nonlocal Cooper Pair Splitting in a pSn Junction, *Phys. Rev. Lett.* **105**, 107002 (2010).
- [15] P. Burset, W. J. Herrera, and A. L. Yeyati, Microscopic theory of Cooper pair beam splitters based on carbon nanotubes, *Phys. Rev. B* **84**, 115448 (2011).
- [16] K. Sato, D. Loss, and Y. Tserkovnyak, Crossed Andreev reflection in quantum wires with strong spin-orbit interaction, *Phys. Rev. B* **85**, 235433 (2012).
- [17] H. Soller and A. Komnik, P-wave Cooper pair splitting, *Beilstein J. Nanotechnol.* **3**, 493 (2012).
- [18] A. Cottet, Microwave spectroscopy of a Cooper pair beam splitter, *Phys. Rev. B* **86**, 075107 (2012).
- [19] V. Giovannetti and K. Yuasa, Probing Cooper pairs with Franck interferometry, *Phys. Rev. B* **86**, 115429 (2012).
- [20] D. Loss and E. V. Sukhorukov, Probing Entanglement and Nonlocality of Electrons in a Double-Dot via Transport and Noise, *Phys. Rev. Lett.* **84**, 1035 (2000).
- [21] D. Chevallier, J. Rech, T. Jonckheere, and T. Martin, Current and noise correlations in a double-dot Cooper-pair beam splitter, *Phys. Rev. B* **83**, 125421 (2011).
- [22] J. Rech, D. Chevallier, T. Jonckheere, and T. Martin, Current correlations in an interacting Cooper-pair beam splitter, *Phys. Rev. B* **85**, 035419 (2012).
- [23] A. Di Lorenzo and Y. V. Nazarov, Full Counting Statistics with Spin-Sensitive Detectors Reveals Spin Singlets, *Phys. Rev. Lett.* **94**, 210601 (2005).
- [24] J. P. Morten, D. Huertas-Hernando, W. Belzig, and A. Brataas, Elementary charge transfer processes in a superconductor-ferromagnet entangler, *EPL* **81**, 40002 (2008).
- [25] H. Soller, L. Hofstetter, and D. Reeb, Entanglement witnessing in superconducting beamsplitters, *EPL* **102**, 50009 (2013).
- [26] F. Brange, O. Malkoc, and P. Samuelsson, Minimal Entanglement Witness from Electrical Current Correlations, *Phys. Rev. Lett.* **118**, 036804 (2017).
- [27] N. M. Chtchelkatchev, G. Blatter, G. B. Lesovik, and T. Martin, Bell inequalities and entanglement in solid-state devices, *Phys. Rev. B* **66**, 161320(R) (2002).
- [28] P. Samuelsson, E. V. Sukhorukov, and M. Büttiker, Orbital Entanglement and Violation of Bell Inequalities in Mesoscopic Conductors, *Phys. Rev. Lett.* **91**, 157002 (2003).
- [29] A. Bednorz and W. Belzig, Proposal for a cumulant-based Bell test for mesoscopic junctions, *Phys. Rev. B* **83**, 125304 (2011).
- [30] B. Braunecker and P. Simon, Interplay Between Classical Magnetic Moments and Superconductivity in Quantum One-Dimensional Conductors: Toward a Self-Sustained Topological Majorana Phase, *Phys. Rev. Lett.* **111**, 147202 (2013).
- [31] W. Kłobus, A. Grudka, A. Baumgartner, D. Tomaszewski, C. Schönenberger, and J. Martinek, Entanglement witnessing and quantum cryptography with nonideal ferromagnetic detectors, *Phys. Rev. B* **89**, 125404 (2014).
- [32] S. E. Nigg, R. P. Tiwari, S. Walter, and T. L. Schmidt, Detecting nonlocal Cooper pair entanglement by optical Bell inequality violation, *Phys. Rev. B* **91**, 094516 (2015).
- [33] P. Busz, D. Tomaszewski, and J. Martinek, Spin correlation and entanglement detection in Cooper pair splitters by current measurements using magnetic detectors, *Phys. Rev. B* **96**, 064520 (2017).
- [34] A. Cottet, T. Kontos, and A. L. Yeyati, Subradiant Split Cooper Pairs, *Phys. Rev. Lett.* **108**, 166803 (2012).
- [35] Z. Scherübl, A. Pályi, and S. Csonka, Probing individual split Cooper pairs using the spin qubit toolkit, *Phys. Rev. B* **89**, 205439 (2014).
- [36] F. Brange, K. Prech, and C. Flindt, Dynamic cooper pair splitter, *Phys. Rev. Lett.* **127**, 237701 (2021).
- [37] Z. Scherübl, G. Fülöp, C. P. Moca, J. Gramich, A. Baumgartner, P. Makk, T. Elalaily, C. Schönenberger, J. Nygård, G. Zaránd, and S. Csonka, Large spatial extension of the zero-energy Yu-Shiba-Rusinov state in a magnetic field, *Nat. Commun.* **11**, 1834 (2020).
- [38] L. Yu, Bound state in superconductors with paramagnetic impurities, *Acta Phys. Sin.* **21**, 75 (1965).
- [39] H. Shiba, Classical spins in superconductors, *Prog. Theor. Phys.* **40**, 435 (1968).
- [40] A. I. Rusinov, On the theory of gapless superconductivity in alloys containing paramagnetic impurities, *Soviet J. Experimental Theoretical Phys.* **29**, 1101 (1969).
- [41] A. V. Balatsky, I. Vekhter, and J.-X. Zhu, Impurity-induced states in conventional and unconventional superconductors, *Rev. Mod. Phys.* **78**, 373 (2006).
- [42] M. R. Buitelaar, T. Nussbaumer, and C. Schönenberger, Quantum Dot in the Kondo Regime Coupled to Superconductors, *Phys. Rev. Lett.* **89**, 256801 (2002).
- [43] A. Eichler, M. Weiss, S. Oberholzer, C. Schönenberger, A. Levy Yeyati, J. C. Cuevas, and A. Martín-Rodero, Even-Odd Effect in Andreev Transport Through a Carbon Nanotube Quantum Dot, *Phys. Rev. Lett.* **99**, 126602 (2007).
- [44] T. Sand-Jespersen, J. Paaske, B. M. Andersen, K. Grove-Rasmussen, H. I. Jørgensen, M. Aagesen, C. B. Sørensen, P. E. Lindelof, K. Flensberg, and J. Nygård, Kondo-Enhanced Andreev Tunneling in InAs Nanowire Quantum Dots, *Phys. Rev. Lett.* **99**, 126603 (2007).
- [45] R. S. Deacon, Y. Tanaka, A. Oiwa, R. Sakano, K. Yoshida, K. Shibata, K. Hirakawa, and S. Tarucha, Tunneling Spectroscopy of Andreev Energy Levels in a Quantum Dot Coupled to a Superconductor, *Phys. Rev. Lett.* **104**, 076805 (2010).
- [46] R. S. Deacon, Y. Tanaka, A. Oiwa, R. Sakano, K. Yoshida, K. Shibata, K. Hirakawa, and S. Tarucha, Kondo-enhanced Andreev transport in single self-assembled InAs quantum dots contacted with normal and superconducting leads, *Phys. Rev. B* **81**, 121308(R) (2010).
- [47] T. Dirks, T. L. Hughes, S. Lal, B. Uchoa, Y.-F. Chen, C. Chialvo, P. M. Goldbart, and N. Mason, Transport through Andreev bound states in a graphene quantum dot, *Nat. Phys.* **7**, 386 (2011).
- [48] B.-K. Kim, Y.-H. Ahn, J.-J. Kim, M.-S. Choi, M.-H. Bae, K. Kang, J. S. Lim, R. López, and N. Kim, Transport Measurement of Andreev Bound States in a Kondo-Correlated Quantum Dot, *Phys. Rev. Lett.* **110**, 076803 (2013).
- [49] J.-D. Pillet, C. H. L. Quay, P. Morfin, C. Bena, A. Levy Yeyati, and P. Joyez, Andreev bound states in supercurrent-

- carrying carbon nanotubes revealed, *Nat. Phys.* **6**, 965 (2010).
- [50] W. Chang, V. E. Manucharyan, T. S. Jespersen, J. Nygård, and C. M. Marcus, Tunneling Spectroscopy of Quasiparticle Bound States in a Spinful Josephson Junction, *Phys. Rev. Lett.* **110**, 217005 (2013).
- [51] J.-D. Pillet, P. Joyez, R. Žitko, and M. F. Goffman, Tunneling spectroscopy of a single quantum dot coupled to a superconductor: From Kondo ridge to Andreev bound states, *Phys. Rev. B* **88**, 045101 (2013).
- [52] A. Kumar, M. Gaim, D. Steininger, A. L. Yeyati, A. Martín-Rodero, A. K. Hüttl, and C. Strunk, Temperature dependence of Andreev spectra in a superconducting carbon nanotube quantum dot, *Phys. Rev. B* **89**, 075428 (2014).
- [53] J. Schindele, A. Baumgartner, R. Maurand, M. Weiss, and C. Schönberger, Nonlocal spectroscopy of Andreev bound states, *Phys. Rev. B* **89**, 045422 (2014).
- [54] E. J. H. Lee, X. Jiang, M. Houzet, R. Aguado, C. M. Lieber, and S. De Franceschi, Spin-resolved Andreev levels and parity crossings in hybrid superconductor-semiconductor nanostructures, *Nat. Nanotechnol.* **9**, 79 (2014).
- [55] A. Jellinggaard, K. Grove-Rasmussen, M. H. Madsen, and J. Nygård, Tuning Yu-Shiba-Rusinov states in a quantum dot, *Phys. Rev. B* **94**, 064520 (2016).
- [56] E. J. H. Lee, X. Jiang, R. Žitko, R. Aguado, C. M. Lieber, and S. De Franceschi, Scaling of subgap excitations in a superconductor-semiconductor nanowire quantum dot, *Phys. Rev. B* **95**, 180502(R) (2017).
- [57] J. Gramich, A. Baumgartner, and C. Schönberger, Andreev bound states probed in three-terminal quantum dots, *Phys. Rev. B* **96**, 195418 (2017).
- [58] S. Li, N. Kang, P. Caroff, and H. Q. Xu, $0-\pi$ phase transition in hybrid superconductor-insulator nanowire quantum dot devices, *Phys. Rev. B* **95**, 014515 (2017).
- [59] L. Bretheau, J. I.-J. Wang, R. Pisoni, K. Watanabe, T. Taniguchi, and P. Jarillo-Herrero, Tunneling spectroscopy of Andreev states in graphene, *Nat. Phys.* **13**, 756 (2017).
- [60] Z. Su, A. B. Tacla, M. Hocevar, D. Car, S. R. Plissard, E. P. A. M. Bakkers, A. J. Daley, D. Pekker, and S. M. Frolov, Andreev molecules in semiconductor nanowire double quantum dots, *Nat. Commun.* **8**, 585 (2017).
- [61] Z. Su, A. Zarassi, J.-F. Hsu, P. San-Jose, E. Prada, R. Aguado, E. J. H. Lee, S. Gazibegovic, R. L. M. Op het Veld, D. Car, S. R. Plissard, M. Hocevar, M. Pendharkar, J. S. Lee, J. A. Logan, C. J. Palmstrøm, E. P. A. M. Bakkers, and S. M. Frolov, Mirage Andreev Spectra Generated by Mesoscopic Leads in Nanowire Quantum Dots, *Phys. Rev. Lett.* **121**, 127705 (2018).
- [62] Z. Su, R. Žitko, P. Zhang, H. Wu, D. Car, S. R. Plissard, S. Gazibegovic, G. Badawy, M. Hocevar, J. Chen, E. P. A. M. Bakkers, and S. M. Frolov, Erasing odd-parity states in semiconductor quantum dots coupled to superconductors, *Phys. Rev. B* **101**, 235315 (2020).
- [63] J. C. Estrada Saldaña, A. Vekris, V. Sosnovtseva, T. Kanne, P. Krogstrup, K. Grove-Rasmussen, and J. Nygård, Temperature induced shifts of Yu-Shiba-Rusinov resonances in nanowire-based hybrid quantum dots, *Commun. Phys.* **3**, 125 (2020).
- [64] J. C. Estrada Saldaña, A. Vekris, R. Žitko, G. Steffensen, P. Krogstrup, J. Paaske, K. Grove-Rasmussen, and J. Nygård, Two-impurity Yu-Shiba-Rusinov states in coupled quantum dots, *Phys. Rev. B* **102**, 195143 (2020).
- [65] M. Valentini, F. Peñaranda, A. Hofmann, M. Brauns, R. Hauschild, P. Krogstrup, P. San-Jose, E. Prada, R. Aguado, and G. Katsaros, Non-topological zero bias peaks in full-shell nanowires induced by flux tunable Andreev states, *Science* **373**, 82 (2021).
- [66] C. Jünger, R. Delagrè, D. Chevallier, S. Lehmann, K. A. Dick, C. Thelander, J. Klinovaja, D. Loss, A. Baumgartner, and C. Schönberger, Magnetic-Field-Independent Subgap States in Hybrid Rashba Nanowires, *Phys. Rev. Lett.* **125**, 017701 (2020).
- [67] A. García Corral, D. M. T. van Zanten, K. J. Franke, H. Courtois, S. Florens, and C. B. Winkelmann, Magnetic-field-induced transition in a quantum dot coupled to a superconductor, *Phys. Rev. Research* **2**, 012065(R) (2020).
- [68] A. Yazdani, B. A. Jones, C. P. Lutz, M. F. Crommie, and D. M. Eigler, Probing the local effects of magnetic impurities on superconductivity, *Science* **275**, 1767 (1997).
- [69] S.-H. Ji, T. Zhang, Y.-S. Fu, X. Chen, X.-C. Ma, J. Li, W.-H. Duan, J.-F. Jia, and Q.-K. Xue, High-Resolution Scanning Tunneling Spectroscopy of Magnetic Impurity Induced Bound States in the Superconducting Gap of Pb Thin Films, *Phys. Rev. Lett.* **100**, 226801 (2008).
- [70] N. Hatter, B. W. Heinrich, M. Ruby, J. I. Pascual, and K. J. Franke, Magnetic anisotropy in Shiba bound states across a quantum phase transition, *Nat. Commun.* **6**, 8988 (2015).
- [71] G. C. Ménard, S. Guissart, C. Brun, S. Pons, V. S. Stolyarov, F. Debontridder, M. V. Leclerc, E. Janod, L. Cario, D. Roditchev, P. Simon, and T. Cren, Coherent long-range magnetic bound states in a superconductor, *Nat. Phys.* **11**, 1013 (2015).
- [72] M. Ruby, Y. Peng, F. von Oppen, B. W. Heinrich, and K. J. Franke, Orbital Picture of Yu-Shiba-Rusinov Multiplets, *Phys. Rev. Lett.* **117**, 186801 (2016).
- [73] D.-J. Choi, C. Rubio-Verdú, J. de Bruijckere, M. M. Ugeda, N. Lorente, and J. I. Pascual, Mapping the orbital structure of impurity bound states in a superconductor, *Nat. Commun.* **8**, 15175 EP (2017), article.
- [74] L. Cornils, A. Kamlapure, L. Zhou, S. Pradhan, A. A. Khajetoorians, J. Fransson, J. Wiebe, and R. Wiesendanger, Spin-Resolved Spectroscopy of the Yu-Shiba-Rusinov States of Individual Atoms, *Phys. Rev. Lett.* **119**, 197002 (2017).
- [75] G. C. Ménard, S. Guissart, C. Brun, R. T. Leriche, M. Trif, F. Debontridder, D. Demaille, D. Roditchev, P. Simon, and T. Cren, Two-dimensional topological superconductivity in Pb/Co/Si(111), *Nat. Commun.* **8**, 2040 (2017).
- [76] L. Farinacci, G. Ahmadi, G. Reece, M. Ruby, N. Bogdanoff, O. Peters, B. W. Heinrich, F. von Oppen, and K. J. Franke, Tuning the Coupling Of an Individual Magnetic Impurity to a Superconductor: Quantum Phase Transition and Transport, *Phys. Rev. Lett.* **121**, 196803 (2018).
- [77] B. W. Heinrich, J. I. Pascual, and K. J. Franke, Single magnetic adsorbates on s-wave superconductors, *Prog. Surf. Sci.* **93**, 1 (2018).
- [78] S. Kezilebieke, M. Dvorak, T. Ojanen, and P. Liljeroth, Coupled Yu-Shiba-Rusinov states in molecular dimers on NbSe₂, *Nano Lett.* **18**, 2311 (2018).
- [79] L. Schneider, M. Steinbrecher, L. Rózsa, J. Bouaziz, K. Palotás, M. dos Santos Dias, S. Lounis, J. Wiebe, and R. Wiesendanger, Magnetism and in-gap states of 3d transition metal atoms on superconducting Re, *npj Quantum Mater.* **4**, 42 (2019).

- [80] A. Kamlapure, L. Cornils, R. Žitko, M. Valentyuk, R. Mozara, S. Pradhan, J. Fransson, A. I. Lichtenstein, J. Wiebe, and R. Wiesendanger, Investigation of the Yu-Shiba-Rusinov states of a multi-impurity Kondo system, *Nano Lett.* **21**, 6748 (2021).
- [81] O. Peters, N. Bogdanoff, S. Acero González, L. Meliscek, J. R. Simon, G. Reecht, C. B. Winkelmann, F. von Oppen, and K. J. Franke, Resonant Andreev reflections probed by photon-assisted tunnelling at the atomic scale, *Nat. Phys.* **16**, 1222 (2020).
- [82] L. Farinacci, G. Ahmadi, M. Ruby, G. Reecht, B. W. Heinrich, C. Czekelius, F. von Oppen, and K. J. Franke, Interfering Tunneling Paths Through Magnetic Molecules on Superconductors: Asymmetries of Kondo and Yu-Shiba-Rusinov Resonances, *Phys. Rev. Lett.* **125**, 256805 (2020).
- [83] P. Beck, L. Schneider, L. Rózsa, K. Palotás, A. Lászlóffy, L. Szunyogh, J. Wiebe, and R. Wiesendanger, Spin-orbit coupling induced splitting of Yu-Shiba-Rusinov states in antiferromagnetic dimers, *Nat. Commun.* **12**, 2040 (2021).
- [84] D. Wang, J. Wiebe, R. Zhong, G. Gu, and R. Wiesendanger, Spin-Polarized Yu-Shiba-Rusinov States in an Iron-Based Superconductor, *Phys. Rev. Lett.* **126**, 076802 (2021).
- [85] I. Affleck, J.-S. Caux, and A. M. Zagoskin, Andreev scattering and Josephson current in a one-dimensional electron liquid, *Phys. Rev. B* **62**, 1433 (2000).
- [86] B. Probst, F. Domínguez, A. Schroer, A. L. Yeyati, and P. Recher, Signatures of nonlocal Cooper pair transport and of a singlet-triplet transition in the critical current of a double-quantum-dot Josephson junction, *Phys. Rev. B* **94**, 155445 (2016).
- [87] K. Grove-Rasmussen, G. Steffensen, A. Jellinggaard, M. H. Madsen, R. Žitko, J. Paaske, and J. Nygård, Yu-Shiba-Rusinov screening of spins in double quantum dots, *Nat. Commun.* **9**, 2376 (2018).
- [88] M. Aagesen, E. Johnson, C. B. Sorensen, S. O. Mariager, R. Feidenhans, E. Spiecker, J. Nygård, and P. E. Lindelof, Molecular beam epitaxy growth of free-standing plane-parallel InAs nanoplates, *Nat. Nanotechnol.* **2**, 761 (2007).
- [89] M. H. Madsen, P. Krogstrup, E. Johnson, S. Venkatesan, E. Mühlbauer, C. Scheu, C. B. Sørensen, and J. Nygård, Experimental determination of adatom diffusion lengths for growth of InAs nanowires, *J. Cryst. Growth* **364**, 16 (2013).
- [90] H. Shtrikman, R. Popovitz-Biro, A. Kretinin, L. Houben, M. Heiblum, M. Bukaa, M. Galicka, R. Buczko, and P. Kacman, Method for suppression of stacking faults in wurtzite III-V nanowires, *Nano Lett.* **9**, 1506 (2009).
- [91] T. K. S. Wong and S. G. Ingram, Fabrication of sub-20-nm trenches in silicon nitride using CHF₃/O₂ reactive ion etching and oblique metallization, *J. Vacuum Sci. Technol. B* **10**, 2393 (1992).
- [92] J. Gramich, A. Baumgartner, and C. Schönenberger, Sub-gap resonant quasiparticle transport in normal-superconductor quantum dot devices, *Appl. Phys. Lett.* **108**, 172604 (2016).
- [93] G. Fülöp, S. d'Hollosy, A. Baumgartner, P. Makk, V. A. Guzenko, M. H. Madsen, J. Nygård, C. Schönenberger, and S. Csonka, Local electrical tuning of the nonlocal signals in a Cooper pair splitter, *Phys. Rev. B* **90**, 235412 (2014).
- [94] G. Fülöp, F. Domínguez, S. d'Hollosy, A. Baumgartner, P. Makk, M. H. Madsen, V. A. Guzenko, J. Nygård, C. Schönenberger, A. Levy Yeyati, and S. Csonka, Magnetic Field Tuning and Quantum Interference in a Cooper Pair Splitter, *Phys. Rev. Lett.* **115**, 227003 (2015).
- [95] Z. Scherübl, A. Pályi, and S. Csonka, Transport signatures of an Andreev molecule in a quantum dot-superconductor-quantum dot setup, *Beilstein J. Nanotechnol.* **10**, 363 (2019).
- [96] O. Kürtössy, Z. Scherübl, G. Fülöp, I. E. Lukács, T. Kanne, J. Nygård, P. Makk, and S. Csonka, Andreev molecule in parallel inas nanowires, *Nano Lett.* **21**, 7929 (2021).
- [97] <https://doi.org/10.5281/zenodo.5281979>.